

Singlet-to-triplet energy transfer via ${}^1\Pi_1/{}^3\Sigma_1^+$ curve crossings in group 2 and 12 metal-atom/rare-gas systems

Solomon Bililign, Maciej Gutowski,^{a)} Jack Simons, and W. H. Breckenridge
Department of Chemistry, University of Utah, Salt Lake City, Utah 84112

(Received 16 April 1993; accepted 21 May 1993)

Of the excited ${}^1\Pi_1$ electronic states of van der Waals complexes of Mg, Zn, and Cd atoms (M) with rare-gas (RG) atoms, only the Zn·Xe (${}^1\Pi_1$) and Cd·Xe (${}^1\Pi_1$) states predissociate to form the lower-lying triplet states, Zn($4s4p\ {}^3P_2$) and Cd($4s4p\ {}^3P_2$), respectively. It has been postulated that such predissociations occur by means of potential curve crossings between bound ${}^1\Pi_1$ levels and repulsive M·RG (${}^3\Sigma_1^+$) states. Since the M·RG (${}^1\Pi_1$) states become more bound as the RG atom becomes more polarizable, from Ne through Xe, and the M·RG (${}^3\Sigma^+$) states should become more repulsive as the RG atom becomes larger in the same order, the likely reason that only the Zn·Xe and Cd·Xe ${}^1\Pi_1$ states predissociate is that they are the only states which have ${}^1\Pi_1/{}^3\Sigma_1^+$ curve crossings below the energies which are accessed spectroscopically. We have carried out *ab initio* electronic structure calculations using various basis sets, and at various levels of correlation, to examine the repulsive ${}^3\Sigma_1^+$ potential curves of Zn·Ar, Zn·Kr, Zn·Xe, Mg·Ar, and Mg·Xe. These calculations support the general mechanism proposed, and show that the likely reason the Mg·Xe (${}^1\Pi_1$) state does not predissociate is because the ${}^1\Pi_1/{}^3\Sigma_1^+$ curve crossing lies slightly above the energy region probed experimentally. It was necessary to utilize very good quality basis sets and high levels of correlated calculations to obtain agreement with experimental observations. In all cases, there was a regular decrease in the repulsive character of the M·RG (${}^3\Sigma^+$) states as the basis quality and level of correlation was increased.

INTRODUCTION

Group 2 or group 12 metal atoms have ground states with outer-shell ($ns^2\ {}^1S_0$) electronic configurations. Optical promotion of one of these valence electrons into an np -orbital results in excited singlet states with $nsnp\ {}^1P_1$ electronic configurations. Due to the exchange interaction, the corresponding triplet $nsnp\ {}^3P_J$ configurations lie at lower energies. It has now been observed experimentally in several cases that even rare-gas (RG) atoms can sometimes collisionally deactivate the singlet 1P_1 states to the triplet 3P_J states, in violation of the spin conservation rule.¹⁻⁹

Cd·RG systems

Several years ago, Breckenridge and Malmin¹ proposed that deactivation of Cd($5s5p\ {}^1P_1$) to Cd($5s5p\ {}^3P_2$) by rare-gas atoms can occur by means of potential curve crossings between Cd($5s5p\ {}^1P_1$)·RG (${}^1\Pi_1$) states, whose potential curves display wells, and repulsive Cd($5s5p\ {}^3P_2$)·RG (${}^3\Sigma_1^+$) states. Shown in Fig. 1 are the first Cd·Ar states correlating with the singlet (1P_1) and triplet (3P_J) levels of Cd($5s5p$) and the ground-state argon atom.⁹⁻¹³ The curves have either been constructed to fit data from recent laser-induced fluorescence (LIF) experiments on the cold Cd·Ar van der Waals molecule⁹⁻¹³ in a supersonic jet, or estimated from an empirical treatment of spin-orbit coupling.¹³ These potential curves can be understood qualitatively in the following way. Sigma alignment of the Cd($5p$) orbital is more attractive at very long range,

since the axial $5p\sigma$ electron density provides a greater dispersive attraction along the bond axis. However, Cd($5p\sigma$)·Ar($3p\sigma$) electron-electron repulsion also sets in at very large distances, hence the Cd($5s5p\ {}^1P_1$)·Ar(${}^1\Sigma^+$) state is *essentially* repulsive but has a very shallow potential minimum at large R . In contrast, for pi alignment of the Cd($5p$) orbital, the dispersive attraction is *less* at large R , but because the Ar atom is approaching along the $5p\pi$ orbital nodal axis, electron-electron repulsion does not become appreciable until much smaller values of R . The argon atom can thus penetrate closer to the Cd($5s$)⁺ “core,” which is relatively unshielded by the diffuse and transversely aligned Cd($5p\pi$) orbital. The Cd($5s5p\ {}^1P_1$)·Ar(${}^1\Pi_1$) state is therefore much more strongly bound and has a rather small R_e value, as can be seen in Fig. 1.

Similar considerations apply to the lower-lying *triplet* sigma and pi states which correlate with the Cd($5s5p\ {}^3P_J$) + Ar(1S_0) atomic states, but the coupling between spin and orbital angular momentum for such states complicates the picture somewhat.¹³ In the Cd($5s5p\ {}^3P_J$) case, spin-orbit coupling is quite large, and the splitting between the Cd($5s5p\ {}^3P_{0,1,2}$) asymptotic levels can be comparable to or greater than the electrostatic interactions (attraction or repulsion) with Ar at moderate distances R . Thus Hund's case “c” is approached, where the only good quantum number is Ω (Hund's case “a” notation is still used in Fig. 1 to permit comparison with other systems). The states with the same value of Ω (and the same overall parity) strongly interact, and thus can have “mixed” $\pi\pi$ and $p\sigma$ alignment character.¹³⁻¹⁵ The ${}^3\Pi_2$ and ${}^3\Pi_{0+}$ states (see Fig. 1) remain “pure π ” in nature, but the ${}^3\Pi_1$ and ${}^3\Pi_{0-}$ states mix strongly (via the l^+s^- component of the spin-

^{a)}Present address: Department of Chemistry, University of Gdansk, ul. Sobieskiego 18/19, 80-052 Gdansk, Poland.

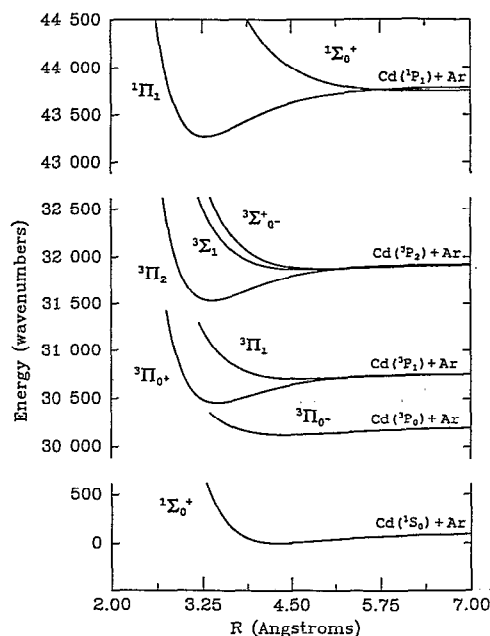


FIG. 1. Morse-function estimates of the potential curves of ground state and the first excited triplet and singlet states of the Cd·Ar van der Waals molecule correlating with Ar($3p^6\ ^1S_0$) and Cd($5s5s\ ^1S_0$), Cd($5s5p\ ^3P_1$), and Cd($5s5p\ ^1P_1$), respectively (Refs. 9–13). Details about the construction of the potentials may be found in Ref. 9.

orbit operator) with the $^3\Sigma_1^+$ and $^3\Sigma_0^+$ states.¹⁶ Because of the *po* character which is therefore mixed into their wavefunctions by the spin-orbit interaction, the latter two $^3\Pi$ states are only quite weakly bound.

At smaller internuclear distances, and much higher energies (comparable to the $^1\Pi_1$ state energies near 43 500 cm^{-1} ; see Fig. 1), where all the triplet states are repulsive, a Hund's case "a" description will be appropriate, since the electrostatic interactions are much greater than the spin-orbit coupling constant. The $^3\Sigma^+$ states are more repulsive than the $^3\Pi$ states at small *R*, and the $^3\Sigma_1^+$ curve could cross the bound $^1\Pi_1$ potential curve. If so, these two states (which both have $\Omega=1$) would be strongly mixed near the crossing region (again, by the l^+s^- component of the spin-orbit operator¹⁶). Thus a Cd($5s5p\ ^1P_1$)·Ar($^1\Pi_1$) state, formed either as an unbound ("full-collision" scattering) species or a bound ("half-collision") state, could easily produce Cd($5s5p\ ^3P_2$)·Ar($^3\Sigma_1^+$) on an outward trajectory, as originally postulated by Breckenridge and Malmin.¹

In the particular case of Cd($5s5p\ ^1P_1$) + Ar, the $^1\Pi_1$ and $^3\Sigma_1^+$ curves do not come close in energy until high on the repulsive inner wall of the $^1\Pi_1$ curve, since the cross section for quenching of Cd($5s5p\ ^1P_1$) by Ar is found to be very low, $<0.01\ \text{\AA}^2$.¹⁻⁴ Laser excitation of bound Cd($5s5p\ ^1P_1$)·Ar($^1\Pi_1$) also results in strong fluorescence, with no predissociation to form Cd($5s5p\ ^3P_2$).¹² Similar conclusions that there are no (low energy) crossings of $^1\Pi_1$ and $^3\Sigma_1^+$ curves can be drawn for the Cd·Ne and Cd·Kr cases. No measurements of Cd(1P_1) collisional deactivation cross sections have been made for Ne or Kr, but the analogous

CdNe($^1\Pi_1$) and CdKr($^1\Pi_1$) states also fluoresce strongly, with no predissociation to form Cd($5s5p\ ^3P_2$).¹²

In contrast, the cross section for the quenching of the Cd($5s5p\ ^1P_1$) state by Xe atoms is quite high, $25 \pm 5\ \text{\AA}^2$,⁵ and the Cd($5s5p\ ^3P_2$) multiplet is the *exclusive* product of the deactivation process; no Cd($5s5p\ ^3P_1$) or Cd($5s5p\ ^3P_0$) were detected.⁵ Consistent with this observation, laser excitation of the cold Cd·Xe van der Waals complex to the Cd($5s5p\ ^1P_1$)·Xe($^1\Pi_1$) state leads to no detectable fluorescence.⁵ However, when a second laser pulse is tuned to detect Cd($5s5p\ ^3P_2$), a series of broadened vibrational transitions is observed which can be assigned to excitation of the strongly predissociated Cd($5s5p\ ^1P_1$)·Xe($^1\Pi_1$) state. Consistent with the full-collision deactivation results, no Cd($5s5p\ ^3P_1$) or Cd($5s5p\ ^3P_0$) populations were detected as predissociation products.⁵ Simulations of the broadened band contours were consistent with Cd·Xe($^1\Pi_1$) bound state lifetimes of only ~ 0.8 ps, indicating predissociation within one vibration.⁵ Such an efficient predissociation is, of course, consistent with the high cross section for collisional deactivation of Cd($5s5p\ ^1P_1$) by Xe atoms.

We believe that the unique behavior of Xe compared to the other RG atoms with regard to singlet-to-triplet deactivation has nothing to do with the "heavy-atom" nature of the Xe atom, which can in some cases increase the effective spin-orbit coupling.^{17,18} After all, Cd($5s5p\ ^1P_1$) is deactivated at essentially every collision by the light H₂ molecule, and the yield of Cd($5s5p\ ^3P_1$) states in this process is known to be quite high ($\sim 30\%$) even when two quite exothermic chemical exit channels are available;^{1,2} the large spin-orbit coupling of the heavy atom Cd($5s5p$) states is thus more than sufficient to induce intersystem crossing.^{19,20} We suggest, instead, that the key question is whether or not the repulsive Cd·RG($^3\Sigma_1^+$) potential curve crosses the attractive Cd·RG($^1\Pi_1$) curve in an energetically accessible region. As one proceeds through the series RG=Ne, Ar, Kr, Xe, the Cd·RG($^1\Pi_1$) states become more *attractive* as the polarizability of the RG atom increases,^{5,12} while the Cd·RG($^3\Sigma_1^+$) states may become more *repulsive* at a given *R* as the hard-sphere radius of the RG atom *increases* in the same series.

Zn·RG systems

This simple idea is quite consistent with the experimental results obtained to date about the interactions of the analogous Zn($4s4p\ ^1P_1$) state with RG atoms. Because of the smaller nuclear charge, the spin-orbit coupling constant for the Zn($4s4p$) states is about three times less than that for the Cd($5s5p$) states. Nevertheless, the trends for RG=Ar, Kr, Xe are remarkably similar to the Cd($5s5p$) cases.^{7,21,22} The cross-sections for deactivation of Zn($4s4p\ ^1P_1$) by Ar or Kr have not been measured, but the bound Zn($4s4p\ ^1P_1$)·Ar($^1\Pi_1$) and Zn($4s4p\ ^1P_1$)·Kr($^1\Pi_1$) van der Waals states fluoresce strongly, with no evidence for predissociation to produce Zn($4s4p\ ^3P_1$) atomic products.^{21,22}

Again, in contrast, no fluorescence is observed after analogous Zn($4s4p\ ^1P_1$)·Xe($^1\Pi_1$) excitation, but when a second laser pulse is fixed in frequency to detect Zn($4s4p$)

3P_2) as a predissociation product, an “action” spectrum is obtained consisting of several vibrational bands with discernible isotopic and broadened rotational structure.⁷ Computer simulations were consistent with $\text{Zn}(5s5p\ ^1P_1) \cdot \text{Xe}(^1\Pi_1)$ predissociation lifetimes on the order of ~ 5 ps, about seven times longer than for the $\text{Cd}(5s5p\ ^1P_1) \cdot \text{Xe}(^1\Pi_1)$ state. There is thus a $^1\Pi_1/{}^3\Sigma_1$ crossing for $\text{Zn} \cdot \text{Xe}$ at energies below the $^1\Pi_1$ vibrational eigenstates of $v'=28$ to $v'=41$ which can be Franck–Condon accessed from the $v''=0$ ground-state (which is the only $\text{Zn} \cdot \text{Xe}$ vibrational state observed in the ultra-cold supersonic expansion). It has been proposed⁷ that the longer predissociation lifetime of $\text{Zn} \cdot \text{Xe}(^1\Pi_1)$ compared to $\text{Cd} \cdot \text{Xe}(^1\Pi_1)$ is due to the lower spin–orbit coupling for Zn vs Cd, since the predissociation rate should depend on the square of the spin–orbit coupling matrix element.¹⁶ Given the correlation⁵ of the efficient predissociation of $\text{Cd} \cdot \text{Xe}(^1\Pi_1)$ with the high cross-section for quenching of $\text{Cd}(5s5p\ ^1P_1)$ by Xe ($\sim 25 \text{ \AA}^2$), we predicted⁷ that the cross-section for the quenching of $\text{Zn}(4s4p\ ^1P_1)$ by Xe would likely be in the 2–5 \AA^2 range. Umemoto and co-workers²³ subsequently measured this cross section experimentally: 3.4 \AA^2 .

Mg · RG systems

Since there are obvious $^1\Pi_1/{}^3\Sigma_1^+$ potential curve crossings in the $\text{Cd} \cdot \text{Xe}$ and $\text{Zn} \cdot \text{Xe}$ cases, one might also expect such a curve crossing for the analogous $\text{Mg}(3s3p\ ^1P_1) \cdot \text{Xe}(^1\Pi_1)$ and $\text{Mg}(3s3p\ ^3P_2) \cdot \text{Xe}(^3\Sigma_1^+)$ states. However, the $\text{Mg}(3s3p\ ^1P_1) \cdot \text{Xe}(^1\Pi_1)$ state has been found to fluoresce strongly, and very careful attempts to detect even small amounts of $\text{Mg}(3s3p\ ^3P_2)$ predissociation product were unsuccessful.²⁴ On the other hand, it is not completely certain whether the very slow predissociation rate is due to the lack of a $^1\Pi_1/{}^3\Sigma_1^+$ curve crossing or to the much lower spin-orbit coupling for the light Mg atom. Assuming the predissociation rate is roughly proportional to the square of the atomic spin–orbit coupling constant for the $nsnp\ ^3P_j$ states, one would predict from the $\text{Zn} \cdot \text{Xe}$ predissociation lifetime a predissociation lifetime for $\text{Mg} \cdot \text{Xe}(^1\Pi_1)$ of ~ 500 ps, which is somewhat shorter than, but of the same order of magnitude as, the $\text{Mg} \cdot \text{Xe}(^1\Pi_1)$ fluorescence lifetime of ~ 2000 ps [presumed to be the same as the free $\text{Mg}(3s3p\ ^1P_1)$ atomic state²⁵].

Ab initio calculations

In all these $\text{M} \cdot \text{RG}$ cases, it is often possible to extract reasonably accurate experimental information about the bound $^1\Pi_1$ potential curves from LIF or action spectroscopy, but such information about the repulsive $^3\Sigma_1^+$ states, especially at several thousand wave numbers above their atomic asymptotic energies where there may be a $^1\Pi_1/{}^3\Sigma_1^+$ crossing, is virtually impossible to obtain experimentally. We have therefore performed *ab initio* calculations of these $\text{M} \cdot \text{RG}(^3\Sigma^+)$ repulsive curves for several cases in which the bound $^1\Pi_1$ potential curves have been characterized experimentally, with the goal of examining our general $^1\Pi_1/{}^3\Sigma_1^+$ curve crossing mechanistic ideas as well as providing more information about the cause of the inefficient

TABLE I. Types and exponents of polarization functions (Refs. 28 and 29) added to the Hay–Wadt (Ref. 27) basis set.

		Exponents
Mg	(<i>p</i>)	(0.045, 0.145) ^a
Mg	(<i>d</i>)	(0.115, 0.346) ^b
Zn	(<i>p</i>)	(0.055, 0.176) ^a
Ar	(<i>d</i>)	(0.263, 0.950) ^a
Kr	(<i>d</i>)	(0.182, 0.612) ^a
Xe	(<i>d</i>)	(0.114, 0.365) ^a

^aReference 28.

^bReference 29.

$\text{Mg}(3s3p\ ^1P_1) \cdot \text{Xe}(^1\Pi_1)$ predissociation. The results of these calculations are reported and discussed in this paper.

THEORETICAL METHODOLOGY

The electronic states treated in this paper were described by the quadratic configuration interaction including single and double excitations with approximate treatment of triple excitations based on a self-consistent field (SCF) reference function [QCISD(T)] implemented via the GAUSSIAN 92 code.²⁶ Second, third, and fourth order Møller–Plesset perturbation theory energies (MP2, MP3, MP4) were also computed as checks on our QCISD(T) results.

In all the calculations, the effective core potentials (ECP) basis sets of Hay and Wadt²⁷ were used, and in most calculations higher polarization functions were added to both the metal atom and rare gas atom basis sets. Table I summarizes the types and exponents of the polarization functions added.^{28,29} The *ab initio* calculations were performed using a Sun 670MP workstation.

The RKR potential curves for the $^1\Pi_1$ states were calculated from spectroscopic constants determined experimentally. We used an RKR program³⁰ which incorporates an automated procedure for smoothing to minimize the physically unreasonable behavior which may sometimes arise for the inner branches of RKR potentials, particularly near dissociation limits.

RESULTS AND DISCUSSION

We have performed *ab initio* calculations of the repulsive $^3\Sigma^+$ states of $\text{Mg} \cdot \text{Ar}$, $\text{Mg} \cdot \text{Xe}$, $\text{Zn} \cdot \text{Ar}$, $\text{Zn} \cdot \text{Kr}$, and $\text{Zn} \cdot \text{Xe}$ which correlate with either $\text{Mg}(3s3p\ ^3P)$ or $\text{Zn}(4s4p\ ^3P)$ and the appropriate RG atom. From the experimental observations,⁷ it is virtually certain that the repulsive $\text{Zn}(4s4p\ ^3P_2) \cdot \text{Xe}(^3\Sigma_1^+)$ potential curve crosses the bound $\text{Zn}(4s4p\ ^1P_1) \cdot \text{Xe}(^1\Pi_1)$ potential curve somewhere between the potential minimum of the $^1\Pi_1$ state and $\sim 2450 \text{ cm}^{-1}$ higher in energy ($D_e = 3240 \text{ cm}^{-1}$). It is also likely that the crossing is on the inner wall of the $\text{Zn} \cdot \text{Xe}(^1\Pi_1)$ potential curve, since there is no great variation in predissociation lifetimes for the vibrational levels excited, as would be expected for an outer-wall crossing.^{16,20}

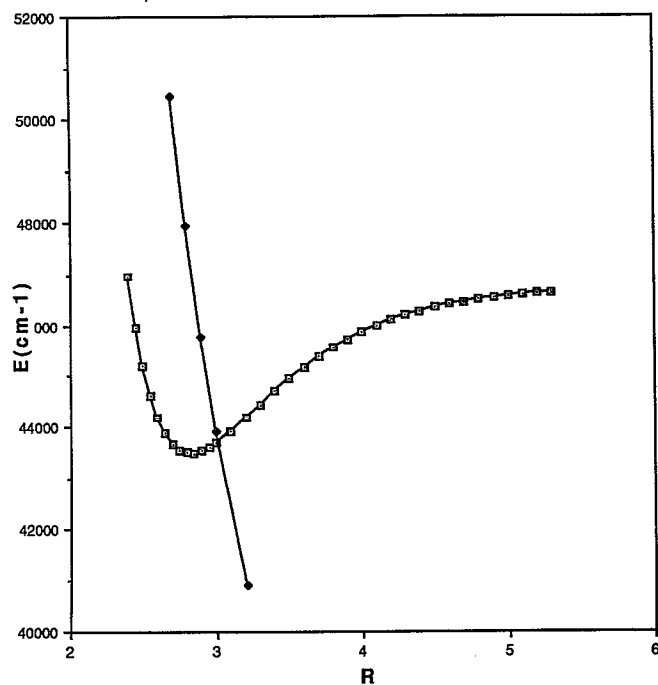


FIG. 2. The repulsive $\text{Zn}(4s4p^3P) \cdot \text{Xe}(^3\Sigma^+)$ state calculated at the SCF level with the Hay-Wadt basis set (Ref. 27). Calculated asymptotic $\text{Zn}(4s4p^3P)/\text{Zn}(4s4s^1S_0)$ energy splitting: 2.78 eV (experimental: 4.05 eV). The energies of the $^3\Sigma^+$ points shown in the figure have been obtained by setting the energy calculated as $R \rightarrow \infty$ to the experimental energy of the $\text{Zn}(4s4p^3P_2)$ state, $32\,890\text{ cm}^{-1}$. Also shown is an RKR potential curve of the $\text{Zn}(4s4p^1P_1) \cdot \text{Xe}(^1\Pi_1)$ state, constructed using spectroscopic constants estimated experimentally (Ref. 7). Internuclear distance R is in Angstroms for this and all figures following.

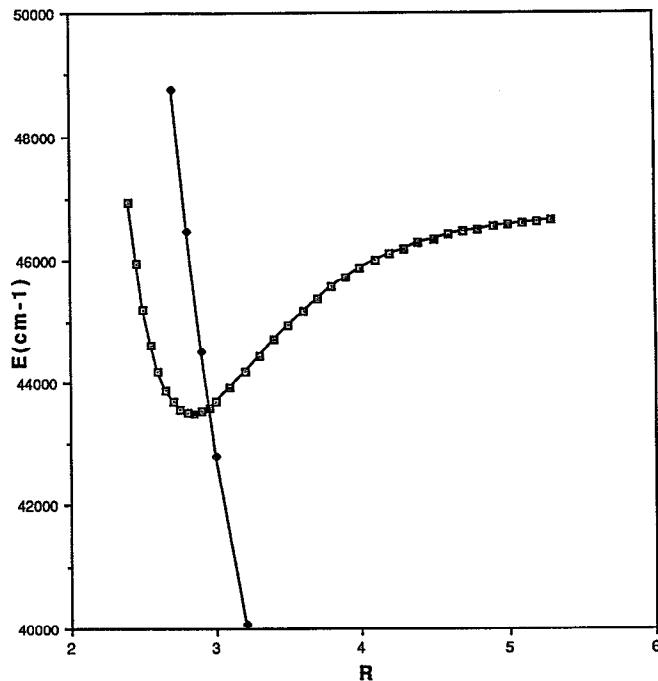


FIG. 3. Same as Fig. 2, except that the calculation of the $^3\Sigma^+$ potential curve was carried out at the MP4 level with the Hay-Wadt basis set (Ref. 27). Calculated asymptotic $\text{Zn}(4s4p^3P)/\text{Zn}(4s4s^1S_0)$ energy splitting: 3.73 eV.

sively less repulsive. For each level of calculation, incremental improvement of the basis set also led to less repulsive character. From the steady decrease in the repulsive nature of the $\text{Zn} \cdot \text{Xe}(^3\Sigma^+)$ potential as the basis set qual-

Zn · RG systems

Shown in Figs. 2, 3, and 4 are results of SCF, MP4, and QCISD(T) *ab initio* calculations of the repulsive $\text{Zn}(4s4p^3P) \cdot \text{Xe}(^3\Sigma^+)$ potential curve. The SCF (Fig. 2) result is usually thought to be of reasonable accuracy for calculation of relative energies of *repulsive* states. Shown also is an RKR potential curve constructed from the experimentally estimated spectroscopic constants for the $\text{Zn}(4s4p^1P_1) \cdot \text{Xe}(^1\Pi_1)$ state.⁷ It can be seen that there is definitely a $^1\Pi_1/{}^3\Sigma_1^+$ crossing, but that the crossing is outer-wall in nature. In Fig. 3, the repulsive $^3\Sigma^+$ curve has been calculated at the correlated MP4 level, but with no polarization functions added to the basis set for either the Zn or the Xe atom. The $^3\Sigma^+$ curve calculated at this level is less repulsive, but the $^3\Sigma_1/{}^1\Pi_1$ crossing is still slightly outer-wall. Finally, in Fig. 4 is shown the $^3\Sigma^+$ curve resulting from the QCISD(T) calculations in which extra *p*-type polarization functions were added to the Zn basis set and extra *d*-type polarization functions to the Xe basis. The $^3\Sigma^+$ curve is even less steeply repulsive, and the $^1\Pi_1/{}^3\Sigma_1^+$ crossing is now "inner-wall," more consistent with the experimental observations.

In fact, as the level of calculation of the $^3\Sigma^+$ states was increased (with the same basis set) from SCF to MP2, MP3, MP4, and QCISD(T), the $^3\Sigma^+$ curves for all Zn · RG and Mg · RG states calculated became progres-

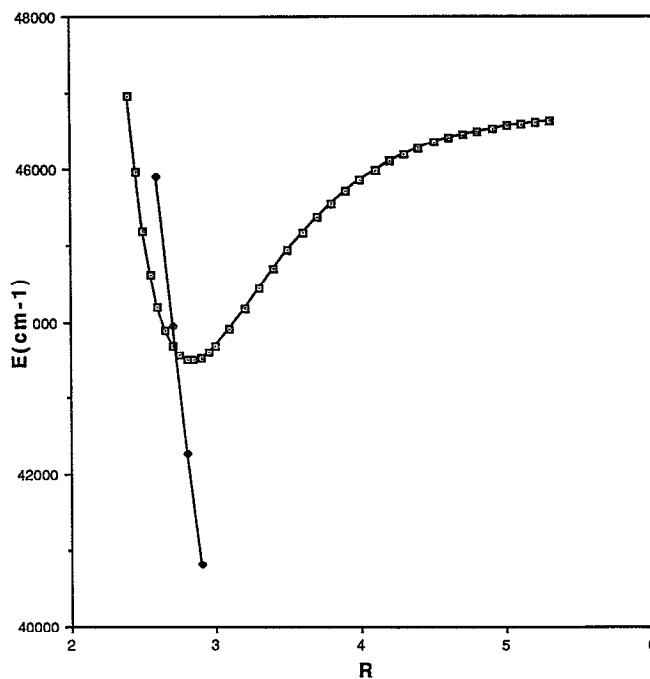


FIG. 4. Same as Fig. 2, except that the calculation of the $^3\Sigma^+$ potential curve was carried out at the QCISD(T) level, with diffuse *p* and *d* functions (see Table I) added to the Hay-Wadt (Ref. 27) basis set. Calculated asymptotic $\text{Zn}(4s4p^3P)/\text{Zn}(4s4s^1S_0)$ energy splitting: 3.92 eV.

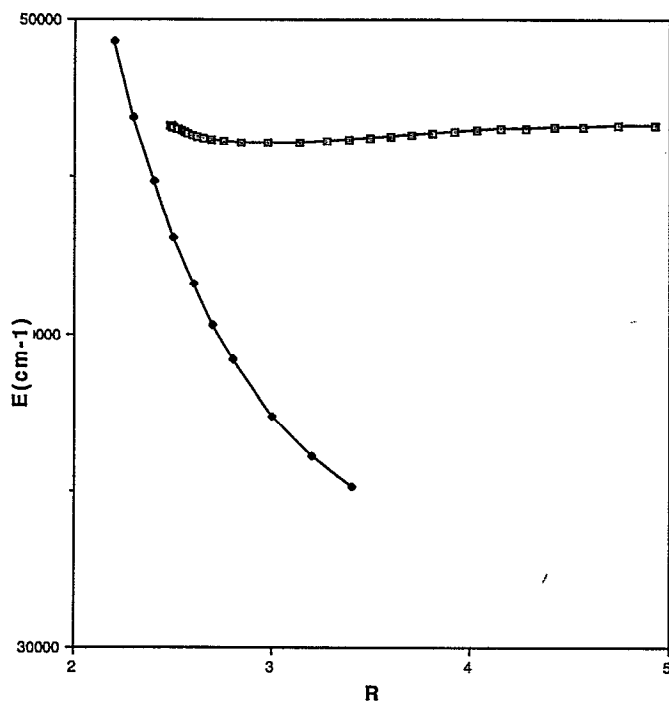
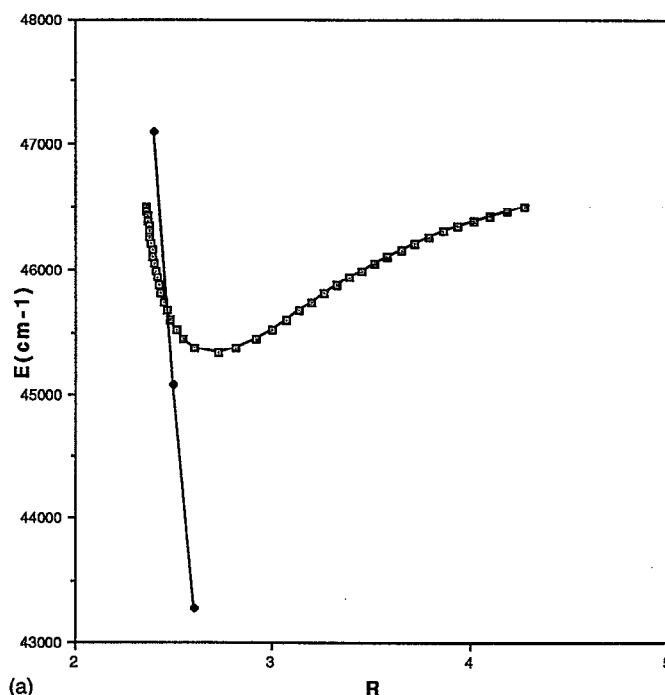


FIG. 5. Same as Fig. 4, except $RG=Ar$; RKR $^1\Pi_1$ potential curve constructed from experimental spectroscopic constants (Ref. 21).

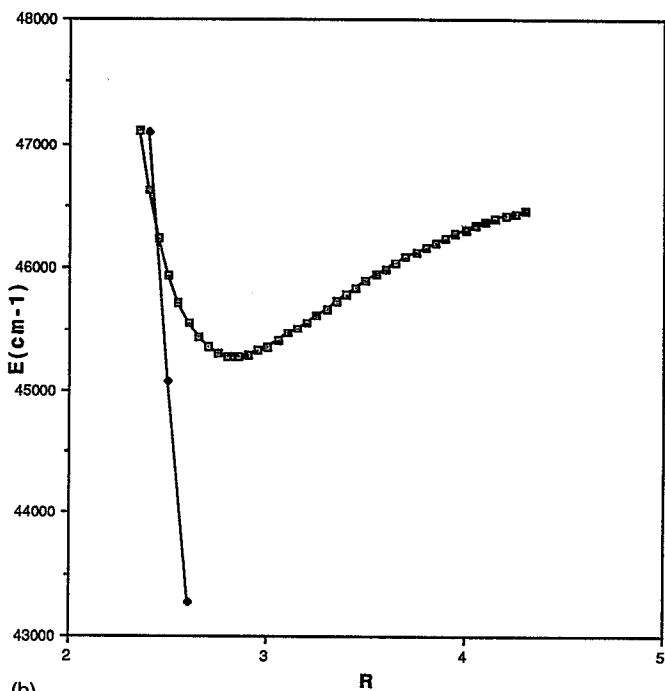
ity and level of the *ab initio* calculation is increased, it appears likely, then, that the *true* $^1\Pi_1/{}^3\Sigma_1^+$ crossing may be even slightly higher in energy on the inner wall of the $^1\Pi_1$ potential curve, which would still be quite consistent, of course, with the experiment results.⁷

Shown in Fig. 5 is a similar QCISD(T) calculation with added polarization functions (see Table I) of the repulsive potential curve of the analogous $Zn(4s4p\ ^3P_2) \cdot Ar(^3\Sigma^+)$ state. In the same figure is an RKR potential curve for the bound $Zn(4s4p\ ^1P_1) \cdot Ar(^1\Pi_1)$ state constructed from the experimentally determined spectroscopic constants.²¹ As can be seen, there is no $^1\Pi_1/{}^3\Sigma_1^+$ curve crossing in the energetically accessible energy region, again consistent with experimental observations.²¹

Shown in Fig. 6(a) is a QCISD(T) calculation with added polarization functions of the repulsive potential curve of the $Zn(4s4p\ ^3P_2) \cdot Kr(^3\Sigma^+)$ state, along with an RKR potential curve of the bound $Zn(4s4p\ ^1P_1) \cdot Kr(^1\Pi_1)$ state constructed from the experimentally determined spectroscopic constants.²² As can be seen, even at the highest level of calculation we have employed, a $^1\Pi_1/{}^3\Sigma_1^+$ inner-wall crossing is predicted. This is *inconsistent* with experimental observations, which show that the $^1\Pi_1/{}^3\Sigma_1^+$ curve crossing cannot occur at energies less than $\sim 46\,500\text{ cm}^{-1}$ [the energy of the highest $Zn \cdot Kr(^1\Pi_1)$ level ($v'=22$) observed in fluorescence]. However, just as in the $Zn \cdot Xe$ case, we observed that as the level of sophistication of the *ab initio* calculation was increased, the $Zn \cdot Kr(^3\Sigma^+)$ state potential curve became less and less repulsive, and it is quite likely that the *true* ${}^3\Sigma^+/{}^1\Pi_1$ curve crossing is indeed above the energy region of the



(a)



(b)

FIG. 6. (a) Same as Fig. 4, except $RG=Kr$; RKR $^1\Pi_1$ potential curve constructed from spectroscopic constants estimated experimentally (Ref. 22). (b) Same as (a) except that the $Zn(4s4p\ ^1P_1) \cdot Kr(^1\Pi_1)$ potential curve is a Morse curve with vibrational spectroscopic constants from Ref. 26, but with $R_e=2.83\text{ \AA}$ [the best-fit value from Franck-Condon simulations (Ref. 22)].

$Zn \cdot Kr(^1\Pi_1)$ potential curve which can be experimentally probed.

Also, since the $Zn \cdot Kr(^1\Pi_1)$ state spectroscopic constants were obtained by computer simulations of overlapped and unresolved isotopic and rotational band structures,²² the uncertainty in the R'_e value (2.74 \AA) of the RKR curve shown in Fig. 6 is probably at least $\pm 0.05\text{ \AA}$.

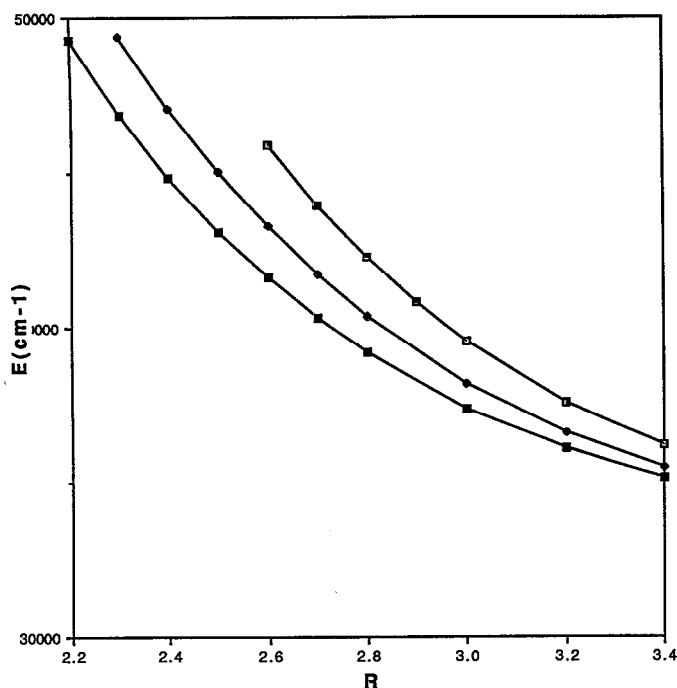


FIG. 7. Calculations of the repulsive $\text{Zn}(4s4p\ ^1P_1) \cdot \text{RG}(^3\Sigma^+)$ states [QCISD(T) level, diffuse p and d functions (see Table I) added to the Hay-Wadt (Ref. 27) basis], where $\text{RG} = \text{Ar}$ (○), Kr (◆), and Xe (□) (see caption to Fig. 4).

A shift of this curve of only $\sim 0.06\ \text{\AA}$ to larger R would be adequate to move the crossing with the calculated $^3\Sigma_1^+$ curve in Fig. 6 to energies greater than $46\ 500\ \text{cm}^{-1}$. In fact, a best-fit Franck-Condon simulation²² of the intensities of the $\text{Zn}(4s4p\ ^1P_1) \cdot \text{Kr}(^1\Pi_1) \leftarrow \text{Zn}(4s4s\ ^1S_0) \cdot \text{Kr}(^1\Sigma^+)$ vibrational transitions resulted in an R_e value for the $^1\Pi_1$ state of $2.83\ \text{\AA}$, almost $0.1\ \text{\AA}$ larger. Shown in Fig. 6(b) is the best-fit Morse curve for the $\text{ZnKr}(^1\Pi_1)$ state, using the same vibrational spectroscopic constants as for the construction of the RKR curve in Fig. 6(a), but with $R_e = 2.83\ \text{\AA}$. There is a crossing, but at $\sim 46\ 500\ \text{cm}^{-1}$, which would be just at the highest vibrational level observed, essentially consistent with experiment.

Shown in Fig. 7 are the QCISD(T) calculations of the repulsive $^3\Sigma^+$ states of $\text{Zn} \cdot \text{Ar}$, $\text{Zn} \cdot \text{Kr}$, and $\text{Zn} \cdot \text{Xe}$ on the same plot. As can readily be observed, the *ab initio* calculations confirm our speculation that the repulsive character at a given R increases as the size of the RG atom increases. In Figure 8, the RKR experimental estimates of the potential curves of the bound $^1\Pi_1$ states of $\text{Zn} \cdot \text{Ar}$, $\text{Zn} \cdot \text{Kr}$, and $\text{Zn} \cdot \text{Xe}$ are shown on the same plot. As can be seen, the well depths increase dramatically as the polarizability of the RG atom increases ($\text{Ar} < \text{Kr} < \text{Xe}$). Perhaps more importantly, however, with regard to the possibility of $^1\Pi_1/{}^3\Sigma^+$ potential curve crossings, the R_e values for the $\text{Zn} \cdot \text{Kr}(^1\Pi_1)$ and $\text{Zn} \cdot \text{Xe}(^1\Pi_1)$ states are essentially identical and even smaller than the R_e value for the $\text{Zn} \cdot \text{Ar}(^1\Pi_1)$ state.

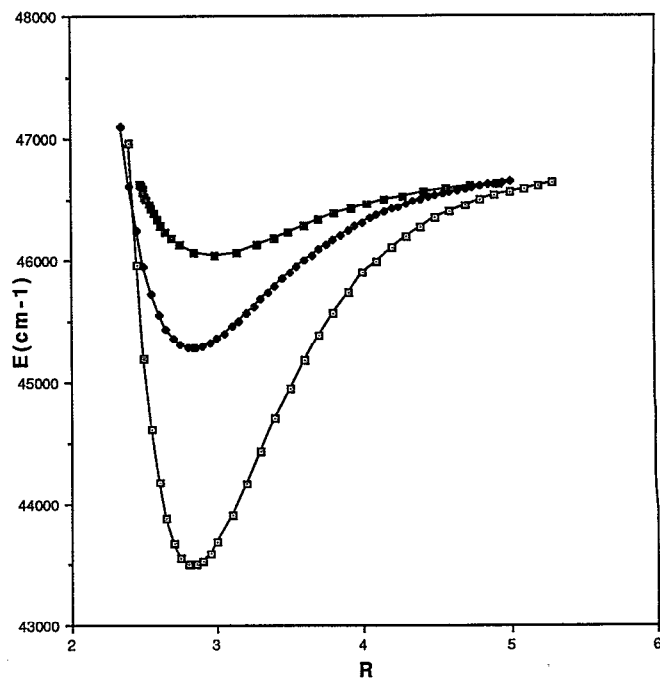


FIG. 8. Estimates of the bound $\text{Zn}(4s4p\ ^1P_1) \cdot \text{RG}(^1\Pi_1)$ potential curves, where $\text{RG} = \text{Ar}$ (○, see Fig. 5 caption), Kr (◆, see Fig. 6(b) caption), and Xe (□, see Fig. 2 caption).

Mg · RG systems

Shown in Fig. 9 are QCISD(T) data for the repulsive $\text{Mg}(3s3p\ ^3P_2) \cdot \text{Ar}(^3\Sigma^+)$ state. Also shown is an RKR potential curve constructed from the experimentally determined spectroscopic constants³¹ of the bound $\text{Mg}(3s3p\ ^1P_1) \cdot \text{Ar}(^1\Pi_1)$ state. There is obviously no low-energy $^1\Pi_1/{}^3\Sigma_1^+$ crossing, consistent with experiment.³¹ In this case, there is no crossing indicated even when the $^3\Sigma^+$ curve is calculated at the SCF level, consistent with the earlier calculations of Boatz, Bak, and Simons.³²

In Fig. 10 are shown results of QCISD(T) calculations for the repulsive $\text{Mg}(3s3p\ ^3P_2) \cdot \text{Xe}(^3\Sigma^+)$ state, as well as an RKR curve constructed from experimentally estimated spectroscopic constants²⁴ for the bound $\text{Mg}(3s3p\ ^1P_1) \cdot \text{Xe}(^1\Pi_1)$ state. As can be seen, a $^1\Pi_1/{}^3\Sigma_1^+$ crossing is indicated, but relatively high on the $\text{Mg} \cdot \text{Xe}(^1\Pi_1)$ inner wall. Again, the $\text{Mg} \cdot \text{Xe}(^3\Sigma^+)$ potential curve became progressively less steeply repulsive as the basis quality and level of *ab initio* method was increased, as shown in Fig. 11. Given this, and in analogy with the ZnKr case, where the experimental result is essentially unambiguous, we believe it is quite likely that the *true* $^1\Pi_1/{}^3\Sigma_1^+$ crossing is somewhat above the highest energy level observed experimentally, $\text{Mg} \cdot \text{Xe}(^1\Pi_1, v' = 20)$ at $\sim 34\ 800\ \text{cm}^{-1}$.²⁴ Also, the RKR curve would only need to be shifted $\sim 0.07\ \text{\AA}$ (an amount probably within the uncertainty in the experimental R'_e value) to larger R for the crossing to occur at $\sim 35\ 000\ \text{cm}^{-1}$. We therefore believe that the most likely explanation for the very slow rate of predissociation of the

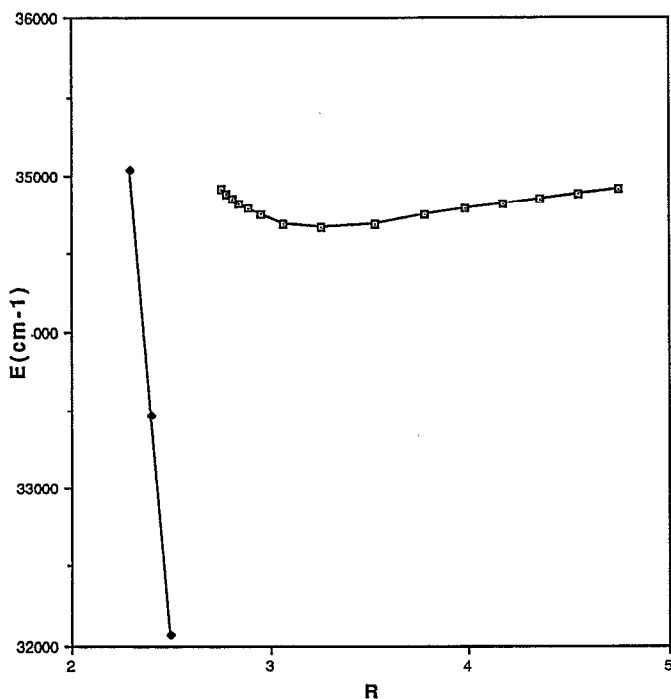


FIG. 9. Calculation of repulsive $\text{Mg}(3s3p^3P) \cdot \text{Ar}(^3\Sigma^+)$ potential curve at the QCISD(T) level, with diffuse p and d functions (see Table I) added to the Hay-Wadt (Ref. 27) basis set. Calculated asymptotic $\text{Mg}(3s3p^3P)/\text{Mg}(3s3s^1S_0)$ energy splitting: 2.54 eV (experimental, 2.71 eV). The bound $\text{Mg}(3s3p^1P_1) \cdot \text{Ar}(^1\Pi_1)$ potential curve shown is an RKR construction from the experimental spectroscopic constants (Ref. 31). The energies of the $^3\Sigma^+$ points in the figure have been obtained by setting the energy calculated as $R \rightarrow \infty$ to the experimental energy of the $\text{Mg}(3s3p^3P_2)$ state, 21 911 cm^{-1} .

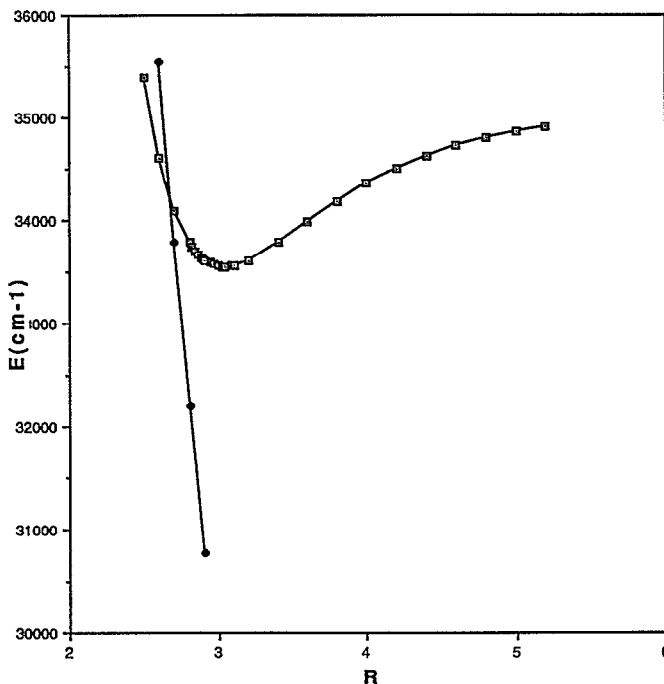


FIG. 10. Same as Fig. 9, except $\text{RG}=\text{Xe}$. The $^1\Pi_1$ RKR curve was constructed from spectroscopic constants estimated experimentally (Ref. 24).

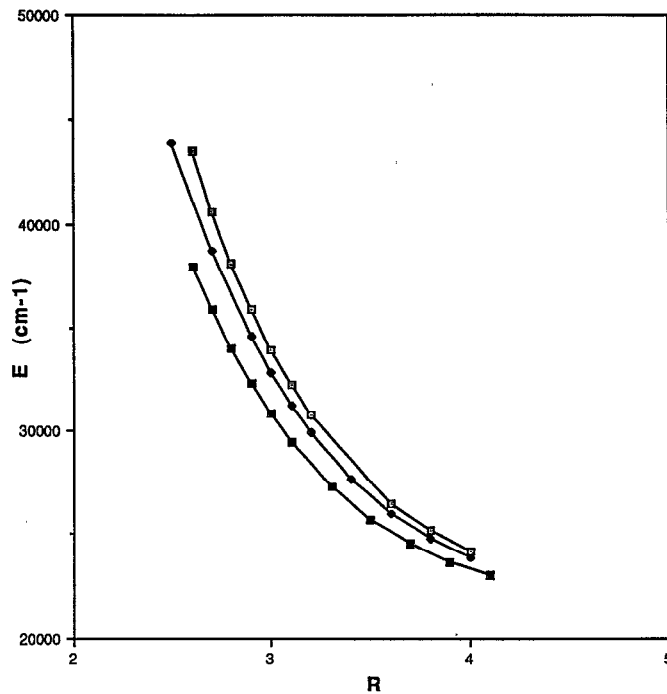


FIG. 11. Calculations of the $\text{Mg}(3s3p^3P) \cdot \text{Xe}(^3\Sigma^+)$ repulsive potential curve done at the SCF level (\square), at the QCISD(T) level with diffuse p functions (see Table I) added to the Hay-Wadt (Ref. 27) basis set on Mg only (\blacklozenge), and at the QCISD(T) level with diffuse p and d functions (see Table I) added to both the Mg and Xe Hay-Wadt (Ref. 27) basis sets (\circ). Again, the energies of the points in each level of calculation are obtained by setting the energy calculated as $R \rightarrow \infty$ to the experimental energy of the $\text{Mg}(3s3p^3P_2)$ state, 21 911 cm^{-1} .

$\text{Mg}(3s3p^1P_1) \cdot \text{Xe}$ state is not low spin-orbit coupling but the fact that the bound $\text{Mg} \cdot \text{Xe}(^1\Pi_1)$ and repulsive $\text{Mg} \cdot \text{Xe}(^3\Sigma_1^+)$ states cross slightly above the energetically accessible energy region.

ACKNOWLEDGMENTS

We are grateful for support of this research by the National Science Foundation, Grants Nos. CHE9215335 (W.H.B.) and CHE9116286 (J.S.), and by the Petroleum Research Fund, Award No. 24573 AC6C (W.H.B.). We thank Professor R. J. LeRoy for kindly providing his RKR program. One of us (S.B.) would like to acknowledge Dr. Alexander Boldyrev for advice and help in using the GAUSSIAN 92 code.

- ¹W. H. Breckenridge and O. Kim Malmin, *J. Chem. Phys.* **74**, 3307 (1981).
- ²W. H. Breckenridge, D. Oba, and W. Nikolai, *J. Phys. Chem.* **90**, 5724 (1986).
- ³W. H. Breckenridge and C. N. Merrow, *J. Chem. Phys.* **88**, 2320 (1988).
- ⁴W. H. Breckenridge and C. N. Merrow, *J. Chem. Phys.* **88**, 2329 (1988).
- ⁵D. J. Funk and W. H. Breckenridge, *J. Chem. Phys.* **90**, 2927 (1989).
- ⁶W. H. Breckenridge, *Acc. Chem. Res.* **22**, 21 (1989).
- ⁷I. Wallace, J. Kaup, and W. H. Breckenridge, *J. Phys. Chem.* **95**, 8060 (1991).
- ⁸I. Wallace, D. J. Funk, J. G. Kaup, and W. H. Breckenridge, in *Gas Phase Metal Reactions*, edited by A. Fontijn (Elsevier, New York, 1992).

- ⁹I. Wallace, Ph.D. thesis, University of Utah, 1991.
- ¹⁰A. Kowalski, M. Czajkowski, and W. H. Breckenridge, *Chem. Phys. Lett.* **121**, 217 (1985).
- ¹¹A. Kvaran, D. J. Funk, A. Kowalski, and W. H. Breckenridge, *J. Chem. Phys.* **89**, 6069 (1988).
- ¹²D. J. Funk, A. Kvaran, and W. H. Breckenridge, *J. Chem. Phys.* **90**, 2915 (1989).
- ¹³R. R. Bennett and W. H. Breckenridge, *J. Chem. Phys.* **96**, 882 (1992).
- ¹⁴R. R. Bennett and W. H. Breckenridge, *J. Chem. Phys.* **92**, 1588 (1990).
- ¹⁵R. R. Bennett, J. G. McCaffrey, and W. H. Breckenridge, *J. Chem. Phys.* **92**, 2740 (1990).
- ¹⁶H. Lefebvre-Brion, R. W. Field, *Perturbations in the Spectra of Diatomic Molecules* (Academic, Orlando, 1986).
- ¹⁷P. Baumann, D. Zimmermann, and R. J. Brühl, *J. Mol. Spectrosc.* **155**, 277 (1992).
- ¹⁸S. P. McGlynn, J. Azumi, and M. Kinoshita, *Molecular Spectroscopy of the Triplet State* (Prentice Hall, New Jersey, 1969).
- ¹⁹I. Wallace, D. J. Funk, J. G. Kaup, and W. H. Breckenridge, *J. Chem. Phys.* **97**, 3135 (1992).
- ²⁰S. Billign, M. D. Morse, and W. H. Breckenridge, *J. Chem. Phys.* **98**, 2115 (1993).
- ²¹I. Wallace, R. R. Bennett, and W. H. Breckenridge, *Chem. Phys. Lett.* **153**, 127 (1988).
- ²²I. Wallace, J. Ryter, and W. H. Breckenridge, *J. Chem. Phys.* **96**, 136 (1992).
- ²³H. Umemoto, T. Ohnuma, H. Ikeda, S. Tsunashima, and K. Kuwahara, *J. Chem. Phys.* **97**, 3282 (1992).
- ²⁴J. G. McCaffrey, D. J. Funk, and W. H. Breckenridge (unpublished).
- ²⁵W. H. Breckenridge and H. Umemoto, *The Dynamics of the Excited State*, edited by K. Lawley, *Advances in Chemical Physics*, Vol. 50 (Wiley, New York, 1982).
- ²⁶J. S. Binkley, M. J. Frisch, D. J. DeFrees, K. Kęghavachri, R. A. Whiteside, H. B. Schlegel, E. M. Fluder, and J. A. Pople, *GAUSSIAN 92* (Carnegie-Mellon University, Pittsburgh, 1992).
- ²⁷W. R. Wadt and P. J. Hay, *J. Chem. Phys.* **82**, 284 (1985); P. J. Hay and W. R. Wadt, *ibid.* **82**, 270 (1985).
- ²⁸J. Andzelm, M. Ktobukowski, E. Radzio-Andzelm, Y. Sakai, and H. Tatewaki, *Gaussian Basis Sets for Molecular Calculations*, edited by S. Huzinaga, *Physical Science Data* 16 (Elsevier, New York, 1984).
- ²⁹R. Ahlrichs, F. Keil, H. Lischka, W. Kutzelnigg, and V. Staemmler, *J. Chem. Phys.* **63**, 455 (1975).
- ³⁰R. J. LeRoy, University of Waterloo Chemical Physics Research Report, 1992.
- ³¹R. R. Bennett, J. G. McCaffrey, I. Wallace, D. J. Funk, A. Kowalski, and W. H. Breckenridge, *J. Chem. Phys.* **90**, 2139 (1990).
- ³²J. A. Boatz, K. L. Bak, and Jack Simons, *Theor. Chim. Acta* **82**, 209 (1992).